Energy and density analyses of the H_2 molecule from the united atom to dissociation: The $^1\Sigma_g^+$ states

Giorgina Corongiu[1,a)] and Enrico Clementi[2]
[1]*Dipartimento di Scienze Chimiche e Ambientali, Università dell'Insubria, via Valleggio 11, I-22100 Como, Italy*
[2]*via Carloni 38, 22100 Como, Italy*

(Received 4 April 2009; accepted 15 June 2009; published online 15 July 2009)

The first 15 $^1\Sigma_g^+$ states of the H_2 molecule are computed with full configuration interaction (CI) both from Hartree–Fock molecular orbitals and Heitler–London atomic orbitals; the computations are correlated with a comprehensive analysis. The basis sets utilized are extended and optimized Slater-type functions [Slater-type orbital (STO)] and spherical Gaussian functions [Gaussian-type orbital (GTO)]. The full CI computations cover the internuclear distances from 0.01 to 10 000 bohr. The available accurate data by Wolniewicz and co-workers for the first five excited states verify the quality of our computations. We focus on the characterization of the orbitals in the wave functions, on the electronic density evolution from the united atom to dissociation, on quantitative decomposition of the total energy into covalent and ionic components, and on detailed analyses of energy contributions to the total state energy from selected STO and GTO subsets. These analyses lead to study (with full CI) the H^- negative ion with a proton and the H^+H^- ion pair systems. The ground and excited states for the He and H atoms and for the H^- ion are computed to discuss the united atom and the dissociation products $H(1s)+H(nl)$ of the n state manifolds. With the exception of $n=1$, each manifold has one state, specifically the *EF*, *H*, 7, and 11, whose second minimum has strong ionic character; state 11 dissociates as H^+H^-. © *2009 American Institute of Physics*.
[DOI: 10.1063/1.3168506]

I. INTRODUCTION

As two hydrogen atoms approach each other a H_2 molecule may be formed. This molecule has a large number of excited states, many experimentally detected and identified.[1–4] Since the beginning of quantum chemistry, the states of H_2, particularly the ground state, have been the subject of many investigations. This is because the H_2 molecule represents the classical and simple test case to verify theoretical quantum mechanical models and computational methods on the stability of molecular systems. In the last decade the H_2 molecule has become the focal point for new technologies to provide clean energy. However, although there has been a lot of computational analysis, the main trust of the theoretical research has tended to focus on the ground and lower excited states rather than on high excited states.

In the 1930s various models[5–8] have been proposed to explain the molecular formation of H_2. Computations of the potential energy curve (PEC), particularly for the ground state, were aimed to test the computational ability to accurately reproduce the laboratory binding energy. An excellent bibliographical survey by McLean *et al.*[9] covers the computations performed in the period of 1927–1960. In 1960 Kolos and Roothaan[10] published the first accurate H_2 calculation. They adopted elliptic coordinates and extended James and Coolidge[11] configuration interaction (CI) computations of the ground state and of a few excited states.[12] The computations for the excited states were soon refined and extended, for example, by Davidson[13] and most notably by Kolos and co-workers (see, for example, Refs. 14–22).

It is now apparent that the James–Coolidge-type expansion in elliptical coordinates is the most reliable technique to obtain accurate potential energy for the ground and excited states of the H_2 molecule. However, almost equal accuracy can be obtained with CI of generalized Gaussian basis sets as demonstrated by Cederbaum and co-workers.[23] They reported small deviations (in the range of 1.82×10^{-4}–5×10^{-5} hartree) from the best Wolniewicz computations in elliptic coordinates.

CI expansions with Gaussian-type orbital (GTO) basis sets using Dunning's cc-pVQZ basis set augmented with diffuse functions have also been considered[24,25] for the first two $^1\Sigma_g^+$ excited states. However, in these publications only graphical PECs are reported, no numerical data are provided, making it difficult to quantitatively assess the accuracy relative to the Kolos–Wolniewicz data. CI expansions and the fully variational MO method with GTO basis sets[26] have been used for computations of four excited states[27] to demonstrate that a relatively short expansion "with full variational optimization"[26] can be equivalent to a larger expansion optimized in the traditional way. When this work was in progress, a study on the $^1\Sigma_g^+$ states 1–7 using the Dunning's cc-pVQZ basis set augmented with diffuse functions has been reported.[28] The errors in the PECs relative to the work of Wolniewicz and co-worker[19,21] are in the range of 1.0×10^{-4}–5.6×10^{-4} hartree. Exponential type basis sets

a)Electronic mail: corongiu@uninsubria.it.

[Slater-type orbital (STO)] have also been used, particularly in the early quantum chemistry publications, e.g., the pioneering work by McLean *et al.*;[9] however, the resulting energies were rather far from Kolos–Wolniewicz-type accuracy, as the basis set was small and the CI expansion was limited to ten configurations.

Although it is now evident that the H_2 ground and several excited states can be computed accurately with James–Coolidge–Kolos CI expansions, the physical interpretation of the resulting wave functions still needs improvements. These are needed, in particular, for the high excited states and for very short and very long internuclear distances. Mulliken,[29] in a pioneering study, proposed interpretations which have been revisited by others more recently.[18–28] These traditional interpretations have been revitalized by a number of important advances, both theoretical and experimental, particularly for the high excited states of H_2 and their interaction with the ion pair H^+H^- (see Refs. 30–33 and the extended literature quoted in these papers). These studies bring new physical concepts and experimental techniques into traditional quantum chemical computations and spectroscopy.

For some of the computed H_2 excited states, questions remain about the reliable identifications of the wave function orbital components. As a consequence, some of the available interpretations of the states appear to call for clarifications, particularly of the role of covalent and ionic character, and the occurrence of the many variations in the electronic density from the vicinity of the united atom to dissociation.

Our work addresses these issues for the first ten $^1\Sigma_g^+$ states and tentatively extends the analyses to the next five excited states. We quantitatively determinate the ionic components in the H_2 states and analyze the contribution of the H and He atomic orbitals (with specific *nl* values) to the H_2 molecule by systematically following the variations in the electronic density. In this work the PECs are computed at the united atom and systematically from $R=0.01$ up to dissociation, as previously reported by Clementi and Corongiu[34] for the H_2 ground state.

An accurate representation of the atomic H and He orbitals is more readily realized with Slater-type exponential functions (a generalization of the hydrogenic orbital functions) than with Gaussian-type functions. Indeed, it has long been recognized that the Periodic Table of elements can be fully explained with models which utilize the orbitals $1s$ to $5f$, thus 14 different *nl* orbitals. These orbitals can be accurately obtained either as numerical tabulations[35] or approximated by short linear combinations of the 14 types of STO functions[36] or with the *generalized* GTO functions[23,37] using a somewhat more extended expansion relative to STO. Traditional GTO functions, being limited to only one *n* value for each *l* value, require more extended linear combinations and make the need of high *nl* value functions more acute.

For excited states, the topic of this work, the above considerations are critical, as we must reproduce the many nodes in the excited state orbitals, particularly in those with high *n* values. Unfortunately, for these *nl* value orbitals the correct representation becomes computationally increasingly problematic when analytical functions, like the STO, or the generalized Gaussian or the Gaussian functions are used.

Since we wish to operate with commonly used basis sets, the above considerations suggest (a) the use of STO to analyze the electronic density and the total energy as a function of basis set relative to the H and He atoms and (b) the use of extended GTO basis sets to check and complement the PECs obtained with STO basis sets. Indeed, the combined use of STO and GTO basis sets allows checks on the accuracy of the computations, particularly useful when eventual extensions of the basis set become computationally problematic. In this work the energy difference resulting from the use of either GTO or STO is between 10^{-4} and 10^{-5} hartree, thus providing a useful check on the computational accuracy, particularly for states where no accurate energy data are available from literature. However, at some internuclear distance intervals in high excited states (7–15), where the component atomic orbitals have high *nl* values (thus many nodes), an extended basis set of GTO outperforms the STO with energy differences up to 10^{-3} hartree. In this work we always specify the type of the adopted basis set.

In conclusion we have opted to use basis sets made either of GTO or STO functions, since familiar to most chemists, even if the corresponding computed energies are generally not as accurate as those obtainable with James–Coolidge–Kolos CI expansions.

Note that in the literature variational computations of excited states often target only one or very few states with basis sets specifically optimized for the root of interest (this simplification finds some theoretical justification in Hylleraas[38] and MacDonald[39]). The drawback of applying this approach to computations of several excited states is that the state orthogonality is no longer guaranteed. For this reason we have constrained our self to use for a defined range of internuclear distances only one basis set for all the 15 states considered.

In Sec. II we provide information on the computational aspect of this work. Section III discusses the electronic density characterization near united atom and dissociation of the 15 $^1\Sigma_g^+$ states and presents a discussion on the PECs for H^- ion interacting with a proton and for the H^+H^- system. In Sec. IV we propose a state correlation diagram for the $^1\Sigma_g^+$ states. In Sec. V, we report on the PECs for the first 15 $^1\Sigma_g^+$ state of H_2, and we compare our computed energies with those reported by Wolniewicz and co-workers for the internuclear separations $R=1.0-100$ bohr. In addition, we complete the presentation of our computed energies for the ground and excited states from the united atom to 1.0 bohr. In Sec. VI we decompose the ground and excited state energies into covalent and ionic components and consider the interactions of H_2 and H^+H^- utilizing the full CI-HL technique (HL denotes Heitler–London). In Sec. VII we analyze the energy of the PECs (multiple minima, depth and position, intersystem crossing, and dissociation) obtained with subsets of the total basis set. In Sec. VIII we systematically identify and analyze the computed electronic density to detail its evolution for each state from the united atom to dissociation; the analysis is reliable for the first six states, reasonable for states 7–10, approximated for the remaining states. Finally, in Sec. IX we summarize the findings of this study.

II. COMPUTATIONAL DETAILS

We restate that our primary goal is the analysis of the wave function electronic densities and energies for the $^1\Sigma_g^+$ states rather than very accurate energy computations (clearly the computed energies must be close to the most accurate literature computations).

For the first time the first ten $^1\Sigma_g^+$ states are analyzed in the full range of internuclear distances, i.e., from the united atom to the dissociation into separated atoms. $R=10\,000$ and 1000 bohr are the largest internuclear separations we have considered. From states 7 to 15 the high nl orbital basis set requirements introduce increasingly convergence difficulties (see below) particularly for the states 11–15; for these five states our analyses are presented as a preliminary study.

Our basis sets are constructed with either GTO or STO functions. Using Dunning's cc-pV6Z basis set[40] $(11s,6p,5d,4f,3g,2h/7s,6p,5d,4f,3g,2h)$ the full CI computation for the ground state at equilibrium separation, 1.4 bohr, yields a total energy of $-1.174\,360$ hartree with a binding of 109.41 kcal/mol. However, the deviations from Wolniewicz's first six $^1\Sigma_g^+$ states are 1.2×10^{-4}, 1.2×10^{-4}, 4.3×10^{-2}, 6.2×10^{-2}, 0.25, and 0.40 hartree, unacceptably large particularly for the high excited states. Therefore, we have experimented with a more extended basis set: 14*s*, 7*p*, 7*d*, 4*f*, 3*g*, and 2*h* uncontracted functions. It yields a ground state total energy of $-1.174\,382$ hartree with a binding energy of 109.43 kcal/mol and deviations of 9.3×10^{-5}, 2.0×10^{-4}, 2.0×10^{-3}, 1.7×10^{-4}, 1.6×10^{-2}, and 1.9×10^{-2} hartree for the first six states. This suggests that improved energies could be obtained with even more extended and carefully optimized basis sets. Indeed, the addition of three *s*, three *p*, and three *d* diffuse functions yields deviations between 7.3×10^{-6} and 5.3×10^{-4} hartree relative to Wolniewicz's data. However, a drawback of this basis set is the frequent occurrence of intruder states when the internuclear distance is varied.

Ideally, the basis set should be optimized at each internuclear distance, pragmatically the same basis set can be kept for a selected interval of internuclear distances. Our STO basis set derives from a "master basis set," which is somewhat modified in four intervals which span the internuclear separation from $R=0$ to 10^4 bohr. Recall that accurate dissociation energies require a STO basis set nicely reproducing hydrogenic functions with $n=1$ to $n=5$ and $l=0$ to $l=3$. However, in the immediate vicinity of the united atom the STO basis set must represent the He ground and excited states; further, proceeding to larger internuclear separations, first, the H_2 molecular repulsive region, then the extended binding region of the $1s^1nl^1$ configurations with multiple minima, requires appropriated and very flexible basis sets.

Our master STO basis set is composed of two 1*s*, three 2*s*, two 3*s*, one 4*s*, one 5*s*, four 2*p*, two 3*p*, one 4*p*, one 5*p*, four 3*d*, one 4*d*, one 5*d*, three 4*f*, and two 5*f* functions. It is used from $R=8$ to 10^4 bohr. The diffuse functions 5*s*, 5*p*, 5*d*, and 5*f* become unnecessary at short internuclear separations; moreover these STOs cause convergence difficulties, thus are omitted from $R=8.0$ to 1.0 bohr. From $R=1.0$ to 0.3 bohr the high nl STO functions must represent the transition from the H_2 molecule to the helium atom, for this reason the 4*f* and 5*f* STOs do require reoptimization. From $R=0.3$ to 0.01 bohr the computations have been performed with the central atom approximation, namely, the helium basis set is centered midway two hydrogen bare nuclei. The latter set of computations leads very smoothly to $R=0$, the He united atom.

From the united atom to $R=0.30$ bohr we have performed computations at 19 internuclear distances clustered particularly near $R=0$. From $R=0.30$ to 0.90 bohr, a region where both energy and density variations are continuous and regular, there are six computations. From $R=0.90$ to 8.0 bohr there are 80 computations and 40 from $R=8.0$ to 100 bohr. From $R=40$ to 100 bohr, the internuclear distances are at intervals of 5 bohr. There are two final computations at $R=1000$ and 10 000 bohr, selected to verify the accuracy of the energy of the separated atoms at dissociation. At 10 000 bohr there is essentially no interaction between the electrons of the two atoms and the nuclear-nuclear repulsion energy is reduced to 1×10^{-4} hartree, a value close to our computational accuracy.

The GTO master basis set is composed of 17*s*, 10*p*, 11*d*, and 7*f* contracted to 12*s*, 10*p*, 8*d*, and 5*f*. The basis set is available upon request to one of us (G.C.). The large number of computations in this work brings about not only a need to secure basis sets appropriated to represent the He and H atoms, the H^- ion, and the H_2 molecule at many internuclear distances, but also the request to select an efficient computational method capable to provide both accuracy in the computed energies and flexibility for decomposition of the wave function into different components. We use both full CI of MO orbitals from Hartree–Fock functions (FCI-HF) and full CI of HL functions (FCI-HL). Recall that for a given basis set, FCI-HF and FCI-HL yield exactly the same total energies but allow different decompositions of the total density. The CI-HL approach has the advantage to allow easy decomposition of the wave function into covalent and ionic contributions and quantitatively clarifies the H_2 connections with the H^+H^- ion pair. In the past, accurate computations on the excited states for H_2 have been performed with classical CI or with multiconfiguration techniques, MC-HF, de facto ignoring the alternative and fully equivalent CI-HL route.

Our nonorthogonal CI code obtains all the needed roots for the ground and excited states directly by diagonalization; therefore the state order is assigned unambiguously. In addition the code accepts both GTO and STO basis sets; for the latter basis the many-center integrals are obtained with the SMILES code.[41] The code features such as computations of HF, HL, HF-HL, MC-HF, MC-HL, and MC-HF-HL wave functions are detailed elsewhere.[42,43]

III. H_2 MOLECULAR PROBABILITY DISTRIBUTION FUNCTIONS AND PECs FOR THE SYSTEMS H^+H^- AND H^- WITH A PROTON

The STO basis is generally recognized to be a good choice for the description of the electronic density in atoms, since specific for *n* and *l* values; further, the exponential form is particularly well suited to represent the cusp region of the *ns* orbitals. For the ground and excited states of the He

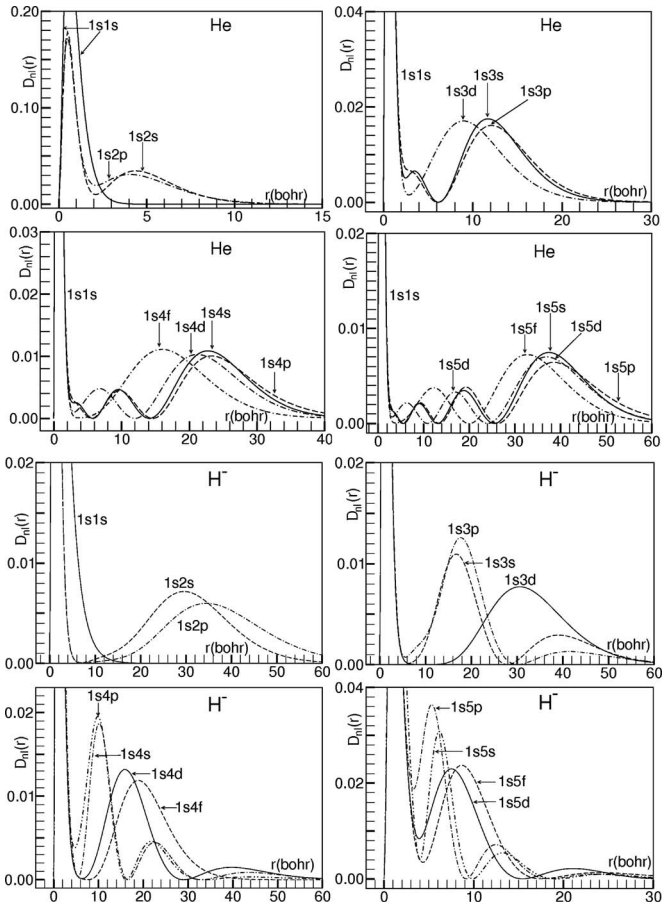

FIG. 1. Comparison of radial distribution function for the configurations $1s^1nl^1$ in the helium atom and in the H^- ion.

atom, the STO basis set is formed by three $1s$, three $2s$, two $3s$, two $4s$, one $5s$, two $6s$, four $2p$, two $3p$, two $4p$, two $5p$, one $6p$, four $3d$, one $4d$, two $5d$, one $6d$, four $4f$, three $5f$, and one $6f$ functions. This basis set yields atomic energies in agreement with the experimental data[44] up to 2×10^{-4} hartree for He$[^1S(1sns)]$, He$[^1P(1snp)]$, He$[^1D(1snd)]$, and He$[^1F(1snf)]$ with n up to 6, but somewhat less accurate for He$[^1S(1s1s)]$, He$[^1D(1s6d)]$, and He$[^1F(1s6f)]$. This basis set is used both for He and for H_2 computations at very short internuclear distances.

As well known, the atomic radial probability distribution functions for the He and H atoms, denoted as $D_{nl}(r)$ (see, for example, Ref. 45), characterize the electronic density evolution at He, the united atom, and at dissociation. The electronic density for each atomic electronic state is characterized and clearly identified by the $D_{nl}(r)$ with node positions and intensity maxima occurring at well defined distances from the nucleus. Starting at the united atom, the characterizations of the He-like orbitals persist in the H_2 molecule at very short distances and progressively evolve into those of the H_2 molecule or of the H^+H^- molecular system and, finally, into those of the H atoms at dissociation. In Fig. 1 we compare the He radial distribution functions for ground and excited states with $1s^1nl^1$ configuration (top four insets) with those of H^- ion (bottom four insets). Note the large shift in the H^- $D_{nl}(r)$ maximum positions relative to those for the He atom and the length of the distribution (even for the ground state, the curve $1s1s$ reaches 15 bohr). In the bottom right inset the $D_{nl}(r)s$ of H^- extend to larger distances than those reported in the figure, but being their intensity too low is graphically poorly visible. The most external maxima in the $1s5s$, $1s5p$, and $1s5d$ configurations are at 44.4, 44.6, and 41.9 bohr, respectively. As expected, for a given $1s^1nl^1$ configuration, the intensity in the negative ion decreases from the maximum at the first node to the following one, whereas the opposite holds for neutral atoms.

One might consider the formation of H_2 either starting from the united atom or, alternatively, from two approaching H atoms. For the H atom the best representation is given by the hydrogenic functions,[45] but good approximation is obtained with linear combinations of STO functions. For the H atom and the H_2 molecule the master STO basis set realistically reproduces the energy of the atomic ground state $^2S(1s)$ and of the atomic excited states $^2S(ns)$, $^2P(np)$, $^2D(nd)$, and $^2F(nf)$ with n up to 5.

In Fig. 2, top insets, we compare the familiar radial distribution functions for the ground and excited states in the H atom (computed with hydrogenic functions) to the combined distributions of $H(1s)$ and $H(nl)$. Recall that the H_2 states in consideration are formed by combining two hydrogen atoms, one in the $^2S(1s)$ ground state and the second in a (nl) excited state. The combination is illustrated with the bottom insets of Fig. 2, where the combined radial distributions of the $1s$ with one nl hydrogenic orbital yield the radial distribution of the molecular $1s^1nl^1$ configuration near dissociation.

Since the density in the H_2 molecule is symmetric upon reflection in the plane perpendicular to the midpoint of the molecular axis (z axis), and since for any given internuclear distance the molecular orbitals are linear combinations of STO basis functions centered at the two nuclear positions, it follows that the knowledge on the STO linear combination at one nuclear position characterizes the electronic density also at the other nuclear position. Further for a given state and for a given internuclear distance R, the STO linear combination generally is characterized by relatively few dominant STO functions.

Recall that the radial distribution function for an atom with wave function $\Psi(r,\theta,\varphi)$ is defined as $D_{nl}(r)=\Psi^2(r)r^2$.[45] We introduce a molecular distribution function devised to represent the probability distribution function for an atom of the molecule along the bond axis; in the following this function is particularly tailored for homonuclear diatomic molecules. For H_2, we consider the electronic density centered on one of the H atoms, set at the origin of the coordinate system (the other atom being at $z=-R$). For a given *state* of H_2 and at a given internuclear distance R, we compute $\Psi^2(0,0,z)z^2$ for a set of z values in the interval 0 to infinity. In analogy with the atomic computations of $D_{nl}(r)$, we consider the function $\Psi^2(0,0,z)z^2$ as an "axial" probability distribution function along the molecular axis for a H atom in H_2. The function is characteristic for a given state and for a given R value and is designated as $D_{\text{state}}(1s,nl)$ or simply state $(1s,nl)$, where "state" stands for one of the 1–15 $^1\Sigma_g^+$ states. Clearly at $R=0$, the $D_{nl}(r)$ for a given helium state coincides with the corresponding state $(1s,nl)$.

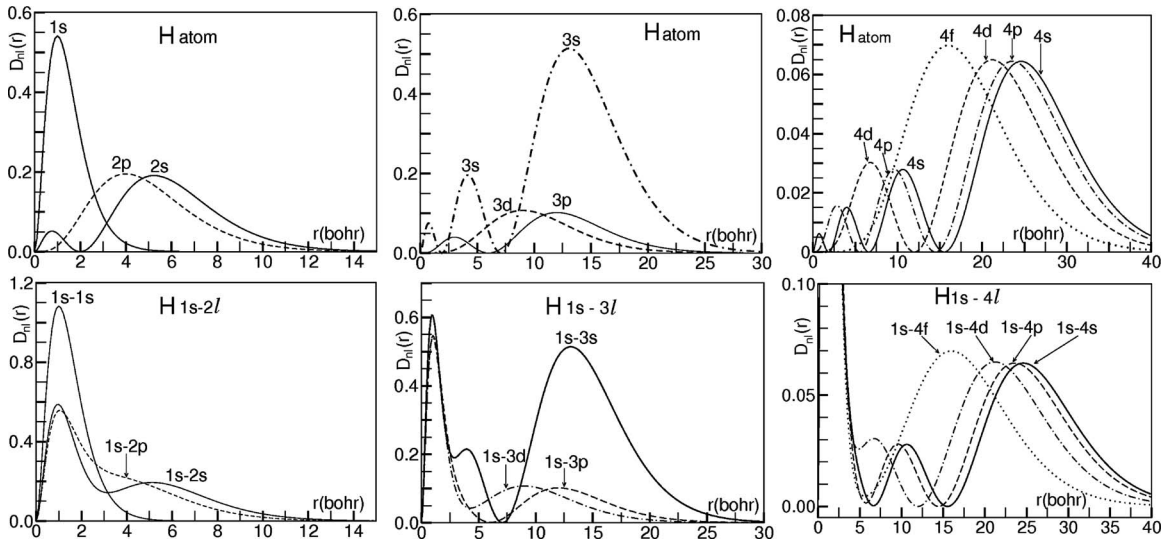

FIG. 2. Atomic radial distribution functions of hydrogenic orbitals for the H atom (top insets) compared to the sum of the atomic radial distribution functions $1s$ and nl (bottom).

In Fig. 3 we provide examples of molecular distribution functions and compare the state $(1s,nl)$ molecular distribution functions for H_2 for states 1–15 with those of H^+H^- discussed later in this work. In the left insets of Fig. 3 we display the molecular $D_{nl}(r)$ for the H^+H^- $[^1S(1s^1nl^1)]$ system near dissociation and we identify for each electronic state 1–14 the configuration at dissociation; thus for example $1(1s'1s')$ in the top left inset indicates electronic state 1, i.e., the H^+H^- ground state, with electronic configuration $1s'^11s'^1$; the configurations are denoted as $1s'1s'$, $1s'2s'$, etc. to differentiate from the notation used for H_2. As expected the atomic $D_{nl}(r)$ of H^- (see Fig. 1) resemble the molecular distributions of the H^+H^- system near dissociation. We compare these distributions to those for H_2 at 10 000 bohr (see the right insets of the figure); note the H^+H^- large shift in the maxima positions. With the help of this type of graphical representation we obtain the characterization of the electronic density for the $^1\Sigma_g^+$ states 1–15, as discussed in Sec. VII.

It is traditional[16,29,46,47] to decompose the H_2 total energy into covalent and ionic contributions; the latter is related to the energy of the H^+H^- system investigated by several authors.[30–33] Concerning the H^- ion it is known that only one state $H^-[^1S(1s^2)]$ is stable. To compute its energy we use the basis set optimized for the H atom; our computed value, −0.527 57 hartree, is not far from −0.527 751 hartree, the accurate computed value by Pekeris.[48]

The H^- ion stabilized in the field of a proton yields a stable H^+H^- system, which can interact with the H_2 system. To asses the stabilization induced on H^- by the proton field we have computed the energy of the etero-nuclear system $H^-[(1s^1nl^1\,]H^+$ with the proton H^+ at variable distances (from 0.1 to 10^4 bohr) from the hydrogen negative ion; the system $H^-[(1s^1nl^1\,]$ with a proton is hereafter denoted as "proton-H^- system," see top inset in Fig. 4. This system has symmetry $C_{\infty v}$ with He states at the united atom and H^- and a proton at dissociation; the minimum energy is −1.133 03 hartree. In this system the binding energy is 1.133 03 −0.527 57=0.605 46 hartree. Note that the path from the united atom to dissociation presents a bifurcation, leading, if symmetry breaking occurs, to the H_2 molecule ground state, which in turn presents a second bifurcation at around 3 bohr, leading either to dissociation into two $H[^2S(1s^1)]$ atoms or to the H^+H^- system. In the top inset of the figure we report also the excited states of the proton-H^- system. We distinguish two, three, and four states with $n=2$, $n=3$, and $n=4$, respectively; note the presence of two minima in the first two excited states.

The H^+H^- system has been previously analyzed; among the many studies we recall, for example, the pioneering works by Herzberg,[1] Mulliken,[29] and Pauling.[47]

In the last few decades, the process of ion formation has been reconsidered; for example, Ref. 31 reports the experiments on radiations on H_2 leading to H^+ and H^-, Ref. 32 discusses the energy threshold for the H^+H^- production, and Ref. 33 presents a study on the dynamics of the H^+H^- system.

We have computed the energies for the homonuclear system H^+H^- $[^1S(1s^1nl^1\,]$, i.e., the H_2 molecular ion pair, hereafter denoted as H^+H^- with $D_{\infty h}$ symmetry imposed as a computational constraint. These energies are from full CI computations, thus include correlation correction. In literature the H^+H^- ground state PEC is often approximated simply by adding to a Coulomb interaction r^{-1} a polarization interaction r^{-4} (see Refs. 21 and 23). This approximation is designated below as "analytic" curve.

The full CI computed ground state energy curve of the H^+H^- system (curve 1 in the bottom inset of Fig. 4) has more structure than the analytic curve and a well defined minimum. The CI curve has energies slightly higher in value than those of H_2 at short distances but then becomes more and more repulsive the larger the internuclear distances (we could say that the HF-MO model which did target the H_2 ground state has de facto approximated the H^+H^- system). As demonstrated by Slater,[46] for the H_2 molecule the HL covalent and ionic functions, although orthogonal at infinity,

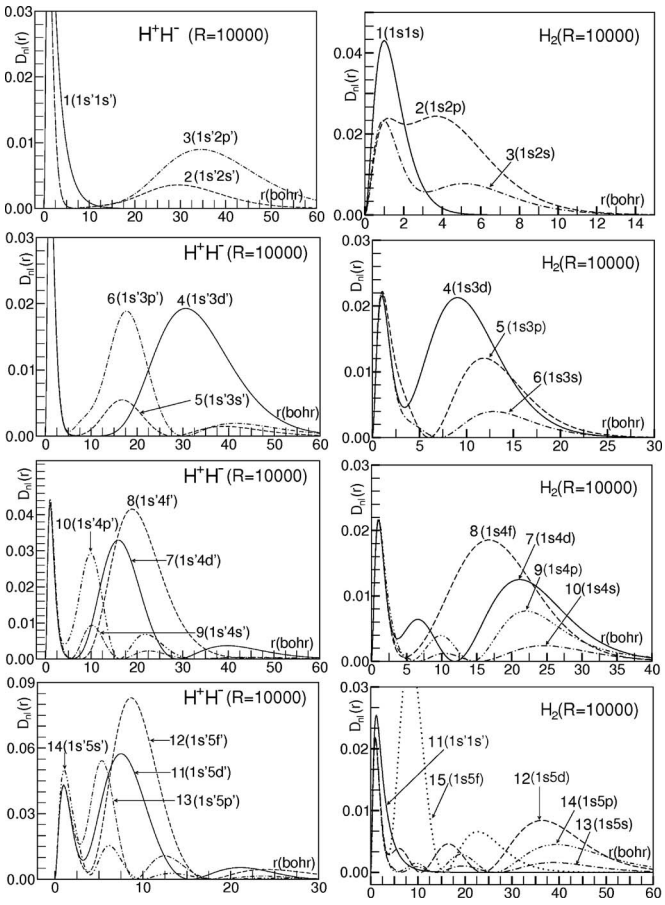

FIG. 3. Molecular distribution functions for the states of the H^+H^- $[1s^1nl^1]$ and the $H_2[1s^1nl^1]$ systems at dissociation.

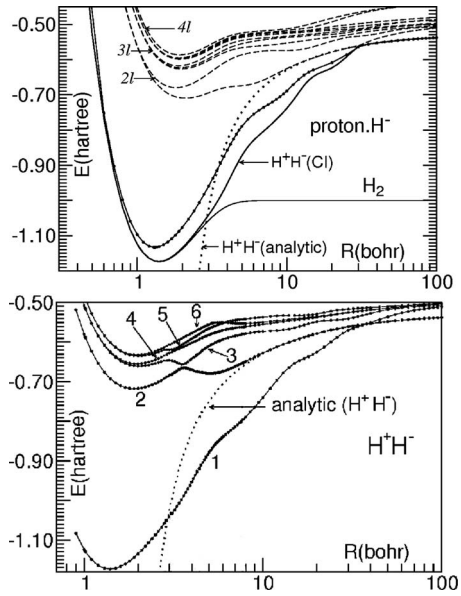

FIG. 4. Computed PECs for the ground and excited states of the proton H^- system $(1s,nl)$ (top) and of the H^+H^- $(1s,nl)$ system (bottom).

are highly nonorthogonal at equilibrium and at shorter distances, actually the shorter the internuclear distance the more the two functions resemble one each other, becoming the same function at the united atom.

We provide a few indicative energy values at different distances for the ion-pair lowest state: at the R values of 10 000, 30, 10, 4, 2, and 1.6 bohr the energies are −0.527 67, −0.570 04, −0.739 76, −0.953 10, −1.135 13, and −1.167 15 hartree, respectively. In addition, note in Fig. 4 the occurrence of multiple minima, particularly for states 2 and 3, at internuclear separations in correspondence of those for the H_2 molecule and the presence of state crossing.

The two systems, proton-H^- and H^+H^-, converge to the same energy value at $R=0$; at the equilibrium distances, $R=1.31$ and $R=1.40$ bohr, respectively, the total energies are −1.133 03 and −1.173 42 hartree, respectively (recall that the H_2 ground state energy at equilibrium, $R=1.40$ bohr, is −1.174 476 hartree). The energies of the two systems are nearly equal from $R=0$ to about $R=0.6$ bohr then differ until around $R=20$ bohr. From here on the energies start to have more and more the same value. The ion pair H^+H^- is computed as more stable than the proton-H^- system; this energy difference is computationally due to the quantum mechanical symmetry constraint present in the ion pair H^+H^- but absent in the proton-H^- system. Recalling that the H atom is less stable than its negative ion, we could interpret the energy loss in proton-H^- as the energy needed to brake the symmetry in H^+H^-, followed by electronic charge transfer from both H atoms to a single H^- ion. The H^+H^- system can cross the proton-H^- system (and vice versa) for a variety of reasons, for example, under the effect of external perturbations capable to brake (or create) symmetry in the system; these perturbations can be due, for example, to radiations, to collision with different molecules, or to interactions on a solid surface, particularly if the latter exhibits ionic character.

The determination of the PECs for the H^+H^- system shows where the H^+H^- states can interact with those of H_2. According to Ref. 30, all the presently observed states of the H^+H^- system fall in the energetic range between $H(1s)+H(3l)$ and $H(1s)+H(4l)$. In Sec. VI we shall return on this topic comparing the excited states of H_2 with those of H^+H^-.

In alternative to the above discussions, the H_2 states can be assumed to be formed by addition of an electron to the H_2^+ molecular ion with configuration $1\sigma_g$ singly occupied, known[1,2] to have a ground state minimum, however, rather far from that of the H_2 ground state. Since long ago, relations between electronic states in H_2 and H_2^+ are available in literature.[1,29,49] Later, in Sec. V, the PEC of the H_2^+ ground state is compared to the PECs of H_2.

IV. STATE AND ORBITAL CORRELATION DIAGRAMS

In diatomic molecules the orbital correlation diagrams are familiar ways[1] to link an orbital of the united atom (placed on the left ordinate axis of the diagram) to an orbital at dissociation (placed on the right ordinate axis), following Wigner–Witmer symmetry correlation rules.[50] The classical correlation diagram builds the molecule either from atomic orbitals of the separated atoms, an implicit application of the HL model, or from orbitals of the united atom, an implicit application of the LCAO-MO model. By filling up with electrons the orbital "correlation segments" (buildup principle)

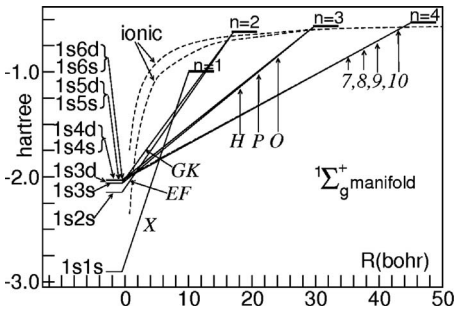

FIG. 5. $^1\Sigma_g^+$ state diagram from the united atom to dissociation (n stands for H[1s]+H[nl]).

the electronic configuration of the molecule is obtained. This procedure is familiar since the classical work by Herzberg.[1] We recall that Mulliken[51] did introduce a somewhat different type of orbital correlation diagram, more informative (but unfortunately more complex) than the standard one,[1] reporting also energy values for the orbitals. Below we present a compromise between the two representations and we describe not only the ground but also the excited states. In other words we present a state correlation diagram rather than an *orbital* correlation diagram to elucidate the gross features of the $^1\Sigma_g^+$ states in the H_2 molecule.

We take full advantage of the fact that we limit ourselves to $1s^1nl^1$ excited states of the H_2 molecule, where one orbital is always 1s and the second is of nl type (with $n \neq 1$ and with a specific l value for each state). Further, whereas in the classical orbital correlation diagram for H_2 only H atoms are considered as dissociation products, we consider both the two H atoms and the H^+H^- pair, which dissociates into H^- with a proton (see Sec. VI).

In Fig. 5 we report a diagram for the ten lowest $^1\Sigma_g^+$ states. In the classical correlation diagram the value of energy for the orbital is not given but simply indicated by giving the relative energy order. In our energy diagram we report for $R=0$ and for dissociation, the computed electronic energy of each state. Thus, the ordinate on the left of the diagram reports the He excited state electronic energies (nearly degenerate for a given n value) and the ordinate at the right reports the H energies. The PECs are approximated as linear interpolation between $R=0$ and dissociation. In addition we report the electronic energy curves for the ground and the first excited state of H^+H^-.

In the classical correlation diagram the distance between united atom and dissociation is simply an indicative connection from united atom to dissociation. In our correlation diagram, the abscissa approximates the H_2 internuclear distance up to dissociation; we start at $R=0$ and end at about $R=45$ bohr. In the figure we note (a) the initial states of the He atom and the final states of the two hydrogen atoms at the dissociation, (b) crossing of states, (c) states very close, thus interacting, (d) the presence of ion-pair energies at rather large internuclear separations and with energy lower than the H_2 dissociation limits, and (e) the suggestion of multiple energy minima as a consequence of state crossing.

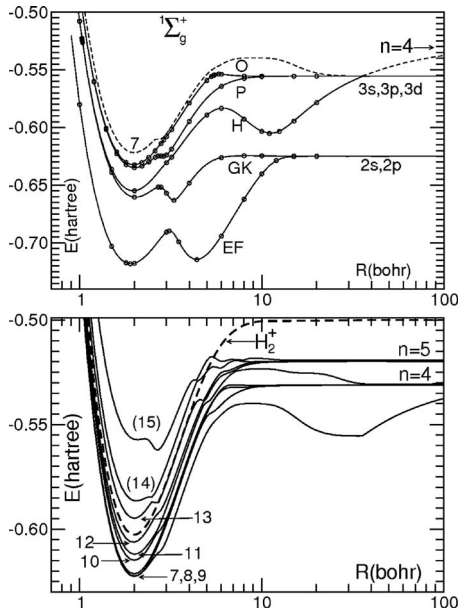

FIG. 6. PECs for $^1\Sigma_g^+$ excited states. Top: states *EF*, *GK*, *H*, *P*, and *O* (solid lines) and state 7 (dashed line); circles sample data from Wolniewicz. Bottom: excited states 7–15 and ground state for H_2^+ (dashed line).

V. COMPUTED ENERGIES

Recall that our computed PECs are obtained both from full HF-CI and full HL-CI; the two methods yield exactly the same PECs as expected. The two sets of eigenfunctions, however, have specific characterizations exploited in our analyses. The use of two basis sets, the STO and GTO, leads to two slightly different sets of computed PECs, since both basis sets are truncated. The energy difference due to the two basis sets is small particularly for the low roots but becomes recognizable for high roots.

Indeed, one would expect that at the united atom and at dissociation the STO basis might yield somewhat better energies than the GTO, whereas for high excited states near the molecular energy minima (approximately in the range of 1–8 bohr), the larger number of GTO functions relative to that of STO might yield a superior representation of orbitals characterizing states with many nodes. In Fig. 6 we display our computed PECs for the $^1\Sigma_g^+$ excited states at internuclear separations between 1 and 100 bohr. The PECs for the states *EF*, *GK*, *H*, *P*, *O*, and 7 reported in the top inset of Fig. 6 are obtained with the STO basis set. The computed PECs for the states 7–15, reported in the bottom inset of the figure, are obtained from the GTO basis set from the internuclear distances of 1.0–8.0 bohr and with STO from 8.2 to 100 bohr. Note that the energies obtained with the two basis sets at the separation distance of 8.0 bohr smoothly merge one into the other, the average energy deviation for the first 15 states is 3.8×10^{-5} hartree.

For state 7 the PEC obtained with the two basis sets is reported twice to facilitate the comparison between the energies from different basis sets, the STO (top inset) and GTO (bottom inset). The energy difference between the STO and the Gaussian basis set computations grows to

TABLE I. First four columns: comparison at R (bohr) near minima (m) and barriers or bumps (b) of total energies E (hartree) from this work and from Wolniewicz and co-worker (Refs. 19 and 21). Fifth and sixth columns: comparison of computed distances (bohr) R_{comp} and R_{expt} for minima from this work and from laboratory data R_{expt}. Last column: total energies E_{expt} obtained from excitation energies of laboratory data (Ref. 2).

State	R[a] (bohr)	E (this work)[b]	E[c]	R_{comp} (this work)[b]	R_{expt} [d]	E_{expt} [d]
E	1.9(m)	−0.718 11	−0.718 146	1.911(m)	1.9120	−0.718 467
EF	3.0 (b)	−0.690 70	−0.690 747		⋯	⋯
F	4.4(m)	−0.714 21	−0.714 518	4.390(m)	4.375	−0.714 691
G	2.0(m)	−0.660 42	−0.660 428	2.030(m)	(2.050)	−0.660 366
GK	2.7 (b)	−0.651v61	−0.651 661		⋯	⋯
K	3.3(m)	−0.662 96	−0.663 102	3.272(m)	(3.33)	(−0.661 118)
H	2.0(m)	−0.654 91	−0.654 926	1.969(m)	(2.013)	−0.655 514
HH	6.2 (b)	−0.583 30	−0.583 424		⋯	⋯
H	11.3(m)	−0.605 13	−0.605 294	11.30 (m)	⋯	⋯
P	2.0(m)	−0.634 88	−0.634 886	2.012(m)	(2.00)	−0.629 852
P	2.7 (b)	−0.624 69	−0.624 709		⋯	⋯
O	2.0(m)	−0.632 42	−0.632 458	1.989(m)	(1.93)	(−0.628 308)
O	5.8 (b)	−0.553 73	−0.553 776		⋯	⋯

[a]Near minimum positions for states 7–14 are at ~2.0 bohr and for state 15 at ~2.7 bohr. States 7 and 10 show a barrier at 8.5 and at 7.0 bohr, respectively.
[b]The computed energies at the first minimum for states 7–12 are −0.622 54, −0.622 33, −0.621 34, −0.614 82, −0.611 99, and −0.606 19, respectively. For states 13–15 the approximated values are −0.594 78, −0.586 43, and −0.562 223 hartree, respectively.
[c]References 19 and 21.
[d]Reference 2.

3×10^{-4} hartree at 2.5 bohr, but the average deviation is 6.2×10^{-5} hartree. The transition between the computed data with the two basis sets is smooth.

In the top inset, the open circles report a representative subset of the energies obtained by Wolniewicz and co-worker;[19,21] for PECs 7–15 no numerical results are available in literature for comparison. The standard state notation adopted by Wolniewicz is kept in the figure.

The energy error for the first five excited states relative to accurate computations[19,21] varies state to state, more precisely, starting from the lowest state, maximum deviations (in hartree) of 3.3×10^{-4} (at $R=5.2$ bohr), 1.6×10^{-4} (at $R=3.1$), 1.9×10^{-4} (at $R=15.0$), 5.5×10^{-5} (at $R=2.9$), and 9.0×10^{-5} (at $R=3.0$). The average deviations are 1.5×10^{-4}, 4.0×10^{-5}, 8.6×10^{-5}, 2.9×10^{-5}, and 3.5×10^{-5}. Note that we have neither considered the relativistic energy corrections[52] smaller than our energy deviations nor the adiabatic energy correction.[19,21]

The energy (in hartree) near minima and the barriers from Corongiu and Clementi and the computations of Wolniewicz and co-worker[19,21] and at the minima from experimental data[2] are compared in Table I. Experimental values in parentheses follow the notation of Ref. 2. For the states 7–10, the minima and eventual barrier are reported as footnote, where we have included, despite the preliminary nature of the assignment, the minimum values for states 11–15, which dissociate as 1s5l. States 13–15 present a minimum but with energy higher than that of the H_2^+ system (dashed line in the bottom inset of Fig. 6). This can be due to limitations of the basis set. On one hand a full representation of the higher quantum number orbitals, particularly $n=5$ and 6, would require additional functions. On the other hand additional extension of the basis set will bring about redundancy problems and appearance of spurious states. For the first 12 states a tabulation of the computed energies at selected internuclear distances is provided in Table II; from $R=0$ to $R=0.6$ bohr we have reported the electronic energy, thereafter the total energy.

In the top inset of Fig. 7 we display our STO computed energies from $R=0$, the helium united atom to $R=0.3$ bohr,

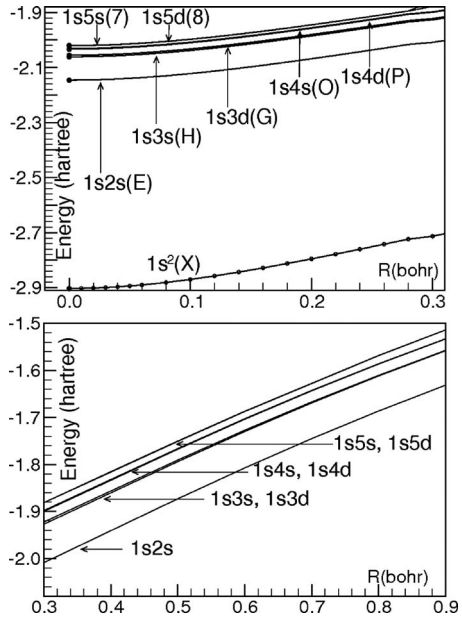

FIG. 7. Computed PECs for the $^1\Sigma_g^+$ states. Top: from $R=0.0$ to $R=0.3$ bohr. Bottom: from $R=0.3$ to $R=0.9$ bohr. Circles (reported only on the ground state curve) mark the internuclear distances in the computations.

TABLE II. Energy values (hartree) at internuclear distances R (bohr) for states 1–12.

	R										
No.	0.00	0.01	0.02	0.10	0.20	0.60	0.80	1.00	1.20	1.40	1.60
1	−2.902 88	−2.902 50	−2.901 39	−2.872 30	−2.801 72	−2.435 96	−1.019 75	−1.124 25	−1.164 66	−1.174 21	−1.168 33
2	−2.145 91	−2.145 63	−2.144 83	−2.123 53	−2.072 45	−1.807 35	−0.436 39	−0.580 05	−0.653 94	−0.691 98	−0.710 30
3	−2.061 25	−2.060 99	−2.060 20	−2.039 30	−1.989 26	−1.729 92	−0.361 79	−0.508 04	−0.585 24	−0.626 51	−0.647 78
4	−2.055 62	−2.055 35	−2.054 58	−2.033 84	−1.984 22	−1.727 26	−0.360 38	−0.507 85	−0.584 26	−0.624 38	−0.644 54
5	−2.033 58	−2.033 31	−2.032 53	−2.011 66	−1.961 86	−1.703 84	−0.336 38	−0.483 27	−0.560 51	−0.601 64	−0.622 73
6	−2.031 28	−2.031 01	−2.030 23	−2.009 47	−1.959 84	−1.702 80	−0.335 85	−0.483 21	−0.560 03	−0.600 67	−0.621 29
7	−2.021 17	−2.020 91	−2.020 13	−1.999 13	−1.949 42	−1.691 90	−0.324 70	−0.471 83	−0.548 88	−0.589 85	−0.610 81
8	−2.020 00	−2.019 74	−2.018 96	−1.998 04	−1.948 40	−1.691 30	−0.324 31	−0.471 62	−0.548 79	−0.589 72	−0.610 59
9	−2.013 94	−2.013 65	−2.012 91	−1.996 69	−1.947 05	−1.689 98	−0.323 00	−0.470 34	−0.547 57	−0.588 62	−0.609 61
10	−2.013 65	−2.013 39	−2.012 61	−1.990 36	−1.940 71	−1.683 59	−0.316 59	−0.463 90	−0.541 10	−0.582 12	−0.603 08
11	−1.997 32	−1.996 90	−1.996 52	−1.989 35	−1.939 54	−1.681 47	−0.314 05	−0.461 06	−0.538 09	−0.579 04	−0.600 02
12	−1.995 74	−1.995 47	−1.994 69	−1.985 65	−1.935 98	−1.678 57	−0.311 28	−0.458 17	−0.534 85	−0.575 28	−0.595 64
No.	1.70	1.90	2.00	2.20	2.40	2.50	2.70	3.00	3.30	3.60	4.00
1	−1.162 21	−1.146 60	−1.137 89	−1.119 89	−1.102 19	−1.093 71	−1.077 81	−1.057 13	−1.040 54	−1.027 89	−1.016 26
2	−0.714 86	−0.718 11	−0.717 68	−0.714 21	−0.708 64	−0.705 44	−0.698 83	−0.690 70	−0.692 26	−0.702 25	−0.711 61
3	−0.653 73	−0.659 60	−0.660 42	−0.659 37	−0.656 25	−0.654 42	−0.651 61	−0.656 84	−0.662 96	−0.657 82	−0.648 11
4	−0.649 93	−0.654 68	−0.654 91	−0.652 59	−0.647 92	−0.645 06	−0.638 89	−0.630 52	−0.623 13	−0.615 25	−0.605 60
5	−0.628 58	−0.634 21	−0.634 88	−0.633 47	−0.629 89	−0.627 79	−0.624 69	−0.623 87	−0.615 57	−0.606 14	−0.594 73
6	−0.626 89	−0.632 02	−0.632 42	−0.630 41	−0.625 96	−0.623 18	−0.617 05	−0.607 93	−0.598 75	−0.589 71	−0.578 80
7	−0.616 58	−0.622 00	−0.622 54	−0.620 85	−0.617 07	−0.614 89	−0.611 43	−0.605 42	−0.595 59	−0.585 96	−0.574 44
8	−0.616 33	−0.621 76	−0.622 33	−0.620 67	−0.616 44	−0.613 72	−0.607 58	−0.597 52	−0.587 37	−0.577 73	−0.566 17
9	−0.615 39	−0.620 81	−0.621 34	−0.619 53	−0.615 20	−0.612 45	−0.606 23	−0.596 07	−0.585 93	−0.576 66	−0.565 53
10	−0.608 85	−0.614 28	−0.614 82	−0.613 05	−0.608 82	−0.606 15	−0.601 50	−0.595 07	−0.585 75	−0.576 13	−0.564 56
11	−0.605 82	−0.611 36	−0.611 99	−0.610 48	−0.606 75	−0.604 55	−0.599 73	−0.589 82	−0.579 72	−0.570 12	−0.558 61
12	−0.601 10	−0.605 93	−0.606 19	−0.603 90	−0.599 27	−0.596 55	−0.592 48	−0.585 68	−0.576 32	−0.567 13	−0.556 08
No.	4.40	4.80	5.20	5.60	5.80	6.20	6.60	7.00	7.60	8.00	9.00
1	−1.009 16	−1.005 05	−1.002 75	−1.001 50	−1.001 10	−1.000 60	−1.000 34	−1.000 19	−1.000 09	−1.000 05	−1.000 02
2	−0.714 21	−0.712 07	−0.707 16	−0.700 84	−0.697 42	−0.690 43	−0.683 52	−0.676 87	−0.667 61	−0.661 97	−0.649 76
3	−0.639 92	−0.633 95	−0.629 99	−0.627 54	−0.626 73	−0.625 66	−0.625 07	−0.624 77	−0.624 58	−0.624 54	−0.624 57
4	−0.597 66	−0.591 59	−0.587 25	−0.584 53	−0.583 75	−0.583 30	−0.584 17	−0.586 04	−0.589 90	−0.592 69	−0.598 99
5	−0.585 23	−0.577 67	−0.571 87	−0.567 55	−0.565 84	−0.563 16	−0.561 20	−0.559 76	−0.558 24	−0.557 53	−0.556 46
6	−0.569 61	−0.562 26	−0.556 89	−0.554 08	−0.553 73	−0.554 04	−0.554 60	−0.555 00	−0.555 32	−0.555 42	−0.555 52
7	−0.564 77	−0.557 06	−0.551 41	−0.547 93	−0.546 60	−0.544 20	−0.542 34	−0.541 12	−0.540 26	−0.540 07	−0.539 99
8	−0.556 37	−0.548 84	−0.544 81	−0.543 07	−0.541 83	−0.539 33	−0.537 31	−0.535 78	−0.534 16	−0.533 40	−0.532 22
9	−0.556 11	−0.548 18	−0.541 76	−0.536 96	−0.535 33	−0.533 20	−0.532 38	−0.532 27	−0.532 30	−0.532 24	−0.532 00
10	−0.554 79	−0.546 93	−0.541 12	−0.536 84	−0.534 97	−0.532 34	−0.531 24	−0.531 05	−0.531 17	−0.531 25	−0.531 34
11	−0.548 82	−0.540 88	−0.538 54	−0.534 61	−0.532 69	−0.529 45	−0.526 97	−0.525 21	−0.524 09	−0.523 87	−0.523 47
12	−0.546 73	−0.539 12	−0.534 40	−0.529 75	−0.528 09	−0.526 20	−0.525 28	−0.524 37	−0.522 80	−0.521 97	−0.520 88
No.	9.50	10.00	11.00	12.00	13.00	20.00	30.00	34.00	50.00	100	10000
1	−1.000 01	−1.000 01	−1.000 00	−1.000 00	−1.000 00	−1.000 00	−1.000 00	−1.000 00	−1.000 00	−1.000 00	−1.000 00
2	−0.644 61	−0.640 11	−0.633 08	−0.628 69	−0.626 47	−0.625 01	−0.625 00	−0.625 00	−0.625 00	−0.625 00	−0.625 00
3	−0.624 61	−0.624 64	−0.624 70	−0.624 74	−0.624 77	−0.624 87	−0.624 96	−0.624 97	−0.624 99	−0.625 00	−0.625 00
4	−0.601 42	−0.603 27	−0.605 09	−0.604 41	−0.601 78	−0.578 27	−0.561 09	−0.557 11	−0.555 55	−0.555 55	−0.555 55
5	−0.556 16	−0.555 97	−0.555 75	−0.555 66	−0.555 61	−0.555 55	−0.555 55	−0.555 55	−0.555 54	−0.555 54	−0.555 54
6	−0.555 52	−0.555 53	−0.555 52	−0.555 52	−0.555 52	−0.555 53	−0.555 53	−0.555 53	−0.555 53	−0.555 52	−0.555 52
7	−0.540 02	−0.540 08	−0.540 40	−0.541 16	−0.542 44	−0.552 79	−0.555 41	−0.555 48	−0.547 58	−0.537 56	−0.531 22
8	−0.531 91	−0.531 76	−0.531 61	−0.531 52	−0.531 46	−0.531 26	−0.531 22	−0.531 22	−0.531 22	−0.531 22	−0.531 20
9	−0.531 85	−0.531 67	−0.531 43	−0.531 33	−0.531 28	−0.531 19	−0.531 17	−0.531 17	−0.531 20	−0.531 20	−0.531 14
10	−0.531 33	−0.531 32	−0.531 29	−0.531 26	−0.531 23	−0.531 16	−0.531 04	−0.531 03	−0.531 15	−0.531 14	−0.530 56
11	−0.523 44	−0.523 42	−0.523 50	−0.523 81	−0.524 32	−0.525 59	−0.529 34	−0.530 30	−0.530 69	−0.530 58	−0.527 66
12	−0.520 58	−0.520 39	−0.520 22	−0.520 15	−0.520 10	−0.519 86	−0.519 77	−0.519 74	−0.519 81	−0.519 88	−0.519 88

and in the bottom inset those from $R=0.3$ to $R=0.9$ bohr. The energy reported in Fig. 7 is the electronic rather than the total energy, a choice made to improve the resolution of the graphic. The figure reports also the energies (bullets) of the He states ($R=0$) and the electronic configurations and labels of the H_2 excited states. The computed internuclear distances are marked as circles only for the lowest state, being tacitly understood that the same set of distances is used for all states. The molecular computed energies clearly connect to specific atomic He energies, and therefore the identification of the origin of the states is unambiguous. Previous studies[19,21] on the excited states have omitted to compute the energy for internuclear separations shorter than 1.0 bohr and used[53] in its place interpolation from the computed values at $R=1.0$ to the He atomic energies. The computed results in Fig. 7 justify the approximation of linear interpolation from $R=1.0$ to the united atom. From 1.0 to 0.6 bohr the interpolation is nearly accurate, then there is a deviation from linearity which varies state to state; for example, in the first excited state the energy deviation is of 0.037 hartree at $R=0.2$ bohr.

From the above data it is apparent that our computed total energies for the first five excited states are quite near to those by Wolniewicz and co-worker;[19,21] for the remaining states the GTO and STO parallel computations provide a realistic check, thus we conclude that our computational accuracy is sufficient to allow a realistic analysis of the energy and electronic density of ground and excited states, the main aim of our work. The "nature" of the wave functions near the united atom can be identified by comparing the atomic radial distribution functions for He ground and excited states (see Fig. 1) to the molecular distribution functions for a hydrogen atom in H_2 (see Sec. III).

The order of the states corresponds to that of the He atom (see Fig. 1) until about $R=1.0$ bohr. In the region, $R=0$ to $R=1.0$ bohr, the molecular wave function changes notably in energy (see Fig. 7) but essentially retains the He atomic character. Changes start to occur after 1.0 bohr, where the electronic configurations for states 3 and 4 as well as for states 5 and 6 interchange due to state crossing. Wolniewicz and Dressler[19] note that in the region $R=1.01$ and $R=1.05$ bohr there is a state crossing between states 3 and 4 and between states 5 and 6. The inspection of our computed energies shows near degeneracy for states 3 and 4 at $R=1.024$ and for states 5 and 6 at $R=1.036$ bohr. In addition, we find near degeneracy for the states 7 and 8 at 1.026 bohr and for states 9 and 10 at 1.014 bohr.

VI. IONIC CHARACTER

Recall that the H^+H^- system can interact with the H_2 states. Let us indicate with $\Psi(H^+H^-)$ the wave functions for the H^+H^- system and with $\Psi(H_2)$ the wave functions for the H_2 system. The $\Psi(H^+H^-)$ is composed by construction only of ionic structures, while the $\Psi(H_2)$ is composed both by covalent and ionic components (structures). Further we recall that the CI-HL energy of $\Psi(H_2)$ can be partitioned into a covalent and an ionic component.

In the top inset of Fig. 8, we compare the total energy for

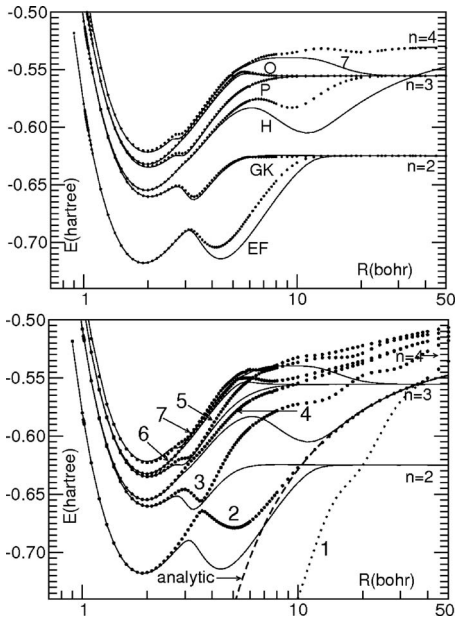

FIG. 8. Excited state PECs. Top inset: total energies for H_2 (full line) compared to covalent energy component (bullets). Bottom inset: total energies for H_2 (full line) and for states of the H^+H^- system (bullets).

the *EF*, *GK*, *H*, *O*, *P*, and 7 states (solid line) with the covalent components (bullets). It is evident that states *E*, *GK*, *P*, and *O* are essentially covalent at all the internuclear distances, whereas states *F*, *H*, and 7 present ionic contributions from about 3, 4, and 7 bohr, respectively, up to dissociation. Only for states *F* and *H* the covalent energy component alone yields a second minimum.

In the bottom inset of Fig. 8, we report again the total energy (solid line) and the energies of the H^+H^- system (bullets) for the corresponding states, the latter designated with numerals 1–7; in the inset we have added for H^+H^- the energies computed with the analytical formula of Ref. 23. Note that the energies of the H^+H^- system have minima at internuclear distances corresponding to those of the H_2 states but differ in the energy, particularly at large distances. In agreement with Refs. 3, 4, and 19, our computations show that the H^+H^- system interacts strongly with the *H* state in the region immediately before dissociation leading to the deep minimum at $R=11.3$ bohr. A similar interaction is responsible for the minimum around $R=33$ bohr for state 7 and for the energy decrease at large distances of state 11 which dissociates as H^+H^- (see Fig. 6). Thus, the states *E*, H, 7, and 11 are strongly affected by the H^+H^- interaction.

A rule emerges by subdividing the excited states into groups with dissociation $H(1s)+H(nl)$ with $n=2,\ldots,5$; for each group there is one state which, in the region of the second minimum, interacts with the H^+H^- system; the higher the value of n the weaker the minimum and the larger the internuclear separation.

For the ground state, the energies of the covalent component coincide with the total energies from infinity to about 8 bohr then show a maximum difference of 0.0013 hartree at 2.0 bohr and finally return to nearly equal values approaching the united atom. The energy difference $E(\text{total})-E(H^+H^-)$ is zero in the proximity of the united atom and

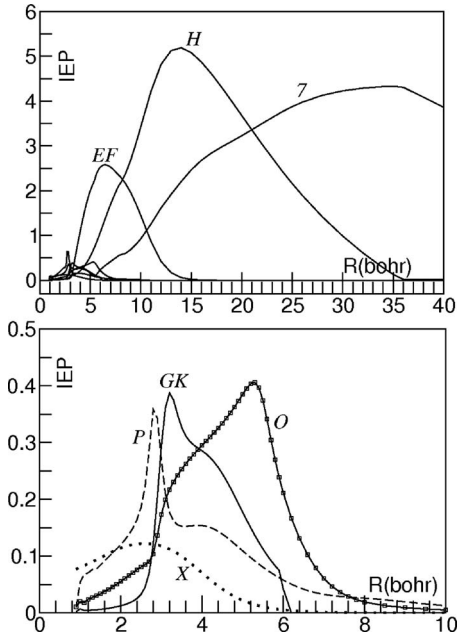

FIG. 9. Top: IEP for ground and excited states from full CI-HL computations. Bottom: details for the states *X*, *GK*, *P*, and *O*.

reaches the values of −0.1, −0.2, −0.4, and −0.5 hartree around 4, 12, 20, and 40 bohr, respectively. Thus, the ground state energy of the H^+H^- system is nearly equal to the H_2 total energy from small *R* values to about $R=2.5$ bohr, then it separates more and more.

To define the ionic character in the PECs of H_2 we introduce the "ionic energy percent" (IEP) concept. The total energy $E(\text{tot})$ and its covalent component $E(\text{cov})$ define a ratio $\eta=E(\text{cov})/E(\text{tot})$, which is nearly 1.0 for predominantly covalent states. The difference $(1.0-\eta)$ is used to define the IEP, $\text{IEP}=100(1-\eta)$; this quantity is zero when the covalent and total energies are equal and 100 when there is no covalent contribution. The computed IEP values are reported in Fig. 9, separated into top and bottom insets because of the very different magnitude of IEP in different states. Note the relatively large values in the second minimum region of states *EF*, *H*, and 7; the nearly symmetrical and narrow region for the *GK* and *O* states, the very localized peak for the *P* state, and the nearly vanishing values for the ground state. The IEP values of the states 8–10 are very small. State 11 after the barrier at about 10 bohr presents a slow energy decay and dissociates with energy equal to the H^+H^- system. In Ref. 23 this feature has been attributed to state 10 (possibly a result of basis set deficiency). According to Ref. 30, all the presently observed states of the H^+H^- system fall in the energetic range between $H(1s)+H(3l)$ and $H(1s)+H(4l)$.

VII. ANALYSIS OF THE PECs VIA BASIS SUBSET DECOMPOSITIONS

In this section we recompute the H_2 PECs using partial rather than full basis set. Note that a subset of basis functions (selected from the full basis set) can represent an orbital in H_2. By reducing the basis set to a few subsets and then by progressively adding the remaining functions from the full

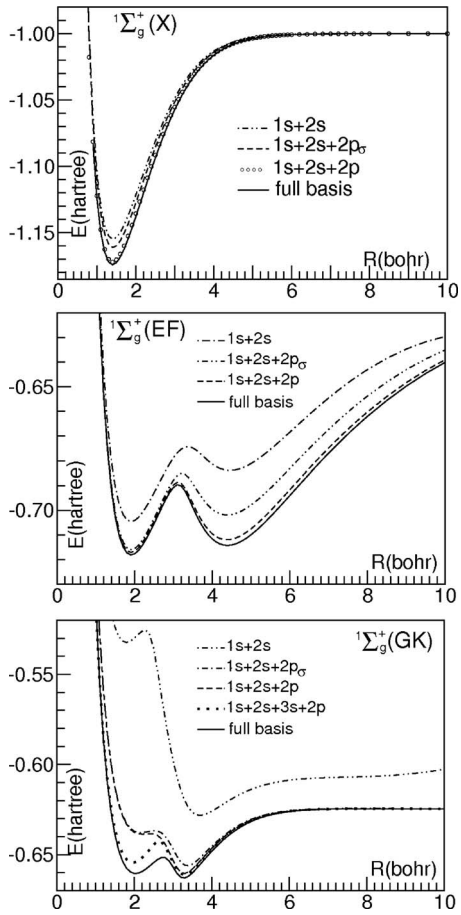

FIG. 10. Subset energy analysis for the *X* (top), *EF* (middle), and *GK* (bottom) states.

basis set we follow in detail (step by step) the formation of the final PEC, and at each step we identify the main contributing orbitals to the PEC.

In the insets of Fig. 10 we consider the *X*, *EF*, and *GK* states. The computed PECs (full line) are compared to those obtained with subsets. The two 1*s* STO functions, the three 2*s* STOs, and the two 3*s* STOs constitute three *s* subsets approximating the 1*s*, 2*s*, and 3*s* orbitals, respectively. Equivalently, the four $2p_\sigma$ and the four $2p_\pi$ STOs constitute two 2*p* subsets.

In the top inset we see that the $1s+2s$ basis subset reproduces the *X* state PEC nearly correctly. The $2p_\sigma$ and $2p_\pi$ subsets add relatively small refinements, whereas the rest of the basis set contribution is negligible.

In the middle inset, the $1s+2s$ subsets approximate the two minima of the *EF* state but at too high energies; at 100 bohr the curve dissociates correctly into $H(1s)+H(2s)$. Finally, the inclusion of the $2p_\sigma$ subset essentially corrects the *E* but not the *F* minimum depth. The $2p_\pi$ subset approximates nearly correctly the *F* minimum.

In the bottom inset the $1s+2s$ subsets yield a state with two minima at approximately the correct internuclear distances of the *GK* minima but too high in energy relatively to the final *GK* PEC. The $2p_\sigma$ subset nearly corrects the depth of the *K* state and notably lowers the energy of the first minimum. The $2p_\pi$ subset reproduces well the K minimum, but the 3*s* subset is needed to reasonably reproduce the *G*

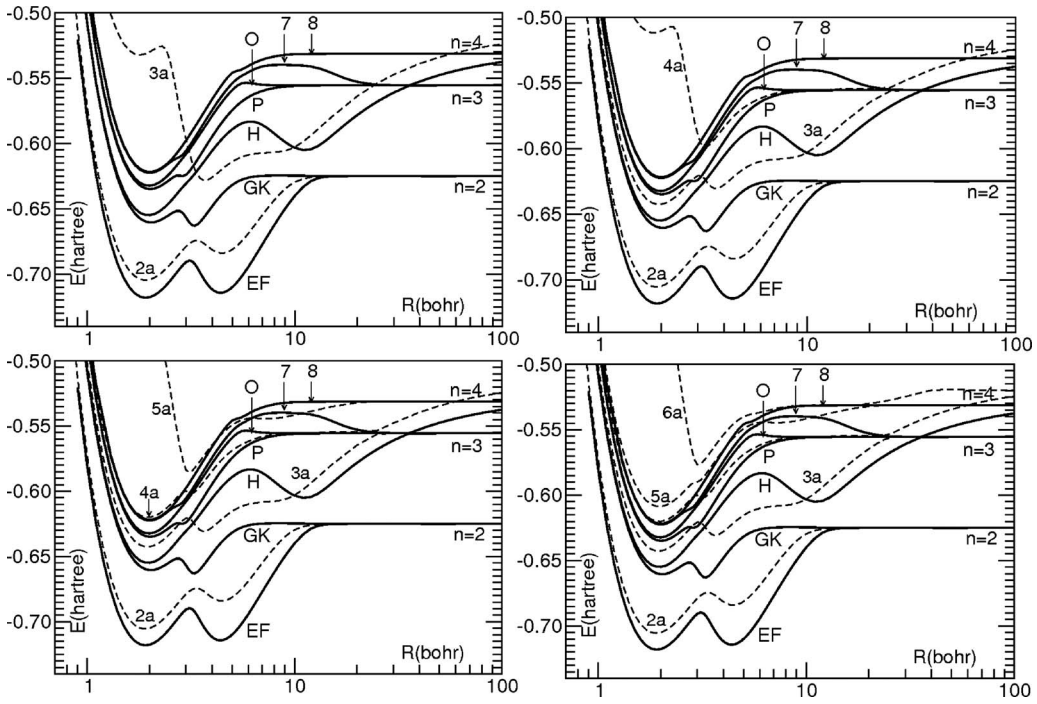

FIG. 11. Comparison between PECs for states 2–8 from full STO basis set (full lines and standard state identification) and from *ns* sub-basis (dashed lines). Top left: $1s+2s$ subsets. Top right: $1s+2s+3s$ subsets. Bottom left: $1s+2s+3s+4s$ subsets. Bottom right: all *ns* subsets.

minimum. Note that the addition of the $2p_\sigma$ functions allows a correct dissociation into $H(1s)+H(2p_\sigma)$. The computations with the full basis set merely refine the quality of the PECs.

From the above subset analysis it is evident that specific energy contributions are linked to the use of specific basis subsets representing specific orbitals. Thus, with this subset analysis we can identify the prevailing *nl* orbitals for a specific state at a specific internuclear separation.

This information can be verified with an analysis on the molecular probability functions of state $(1snl)$ reported in Sec. VIII. Thus, the subset energy analysis of this section and the analysis given in Sec. VIII nicely complement each other.

In Figs. 11–13 we apply the subset energy analysis to all the PECs in the $^1\Sigma_g^+$ state manifold. In the figures the full lines and standard nomenclature identify the final PECs, whereas intermediate computed curves are identified by dashed lines and by the state number identification 1–14, followed by the letter *a* (e.g., $1a, 2a, \ldots, 14a$ for the states $X, EF, \ldots, 14$).

In the top insets of Fig. 11 the 1*s*, 2*s*, and 3*s* subsets generate the states 2*a*, 3*a*, and 4*a* previously discussed in Fig. 10. State 4*a* has two minima, the first one at a very high energy, in correspondence of the *G* and *H* minima, and the second one approximately above the barrier of the *GK* state. We assign the 3*s* orbital, curve 4*a*, as an important orbital needed to generate the minimum of the *G* and of the *H* curves. States 3*a* and 4*a* cross each other at internuclear distances larger than 20 bohr.

In the bottom left inset, after the addition of the 4*s* orbital, the situation does not change for the states 2*a* and 3*a*. The first minimum of state 4*a* becomes deeper and a new state 5*a* appears with a minimum in the region of the barrier of state 4*a*, generated by an avoided crossing between the two states.

In the bottom right inset, after the addition of the 5*s* orbital, the situation remains essentially unchanged for states 2*a*, 3*a*, and 4*a*; state 5*a* presents a deep minimum and a new state 6*a* has a minimum in correspondence of the barrier of state 5*a*, generated by an avoided crossing between the two states. The pairs of states 3*a* and 4*a* and of 5*a* and 6*a* cross each other at about 20 bohr. State 3*a* is higher in energy than state *GK* and the first minimum is also above state *H*; states 4*a*, 5*a*, and 6*a* are higher in energy than the *H*, *P*, and *O* states. The above mentioned crossings bring about the frequent electronic density switching noted in the density analyses (Sec. VIII).

In conclusion the *ns* orbitals in Fig. 11 are the main generators of five minima: 1*a* (not reported for space reason), 2*a*, 3*a*, 4*a*, and 5*a* related to the minima in the *X*, *E*, *G*, *H*, *P*, and *O* states. A second set of minima is generated in the region of the *F* and *K* states; a kink appears in the 5*a* curve related to the *P* state.

No state generated by the full *ns* orbital set fully reproduces the final PECs, even if the overall features of the final PECs can be easily recognized, particularly for the *EF*, *K*, and *H* states. This inability is not surprising: indeed, even the ground state energy is only approximately computed by limiting the basis set to *ns* functions; $2p_\sigma$ and $2p_\pi$ types are needed, less the $3d_\sigma$, $3d_\pi$, $3d_\delta$, etc.

From this figure we have highlighted the importance of state crossing and of state interaction. The drawback of this analysis is the complexity of the resulting plots reported in each inset. On the contrary, the state by state analysis of Fig. 10 is much simpler but omits information relative to state crossing and state interaction.

In the three insets of Fig. 12 we detail the PEC energy variations following the addition of the *np* STO functions to the *ns* STO basis set. The top inset of Fig. 12 reports the

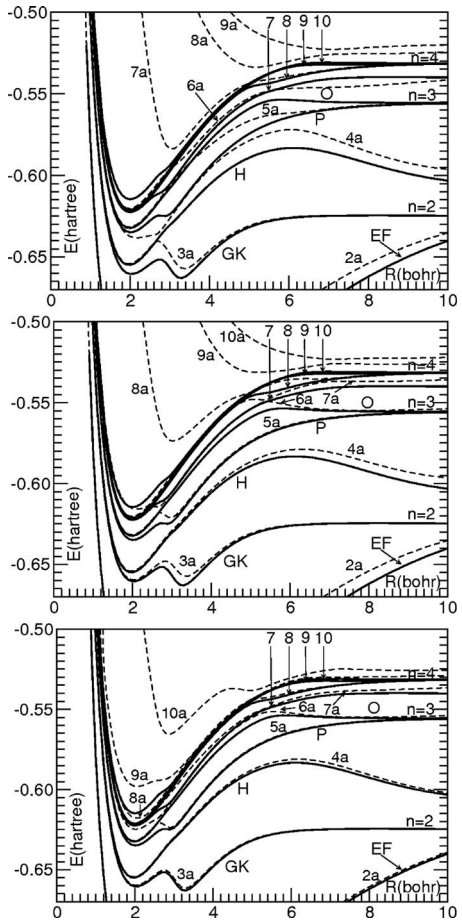

FIG. 12. Comparison between PECs of states 2–10 from full STO basis set (full lines and standard state identification) and from $ns+np$ subsets (dashed lines and na notation with $n=2-10$).Top: $ns+2p_\sigma$ subsets. Middle: $ns+2p_\sigma+3p_\sigma$ subsets. Bottom: $ns+np$ subsets.

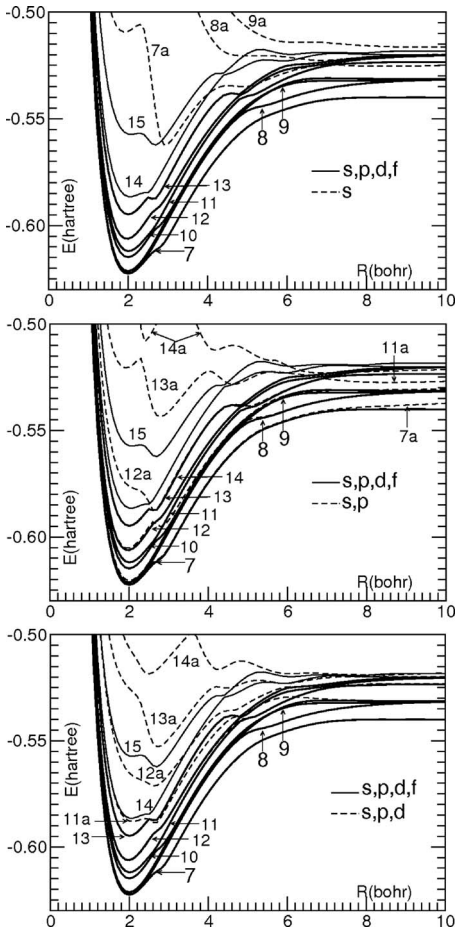

FIG. 13. Comparison between PECs for states 7–15 from full basis set (full lines and standard state identification) and from subsets (dashed lines and na notation with $n=2-14$).Top: ns subsets. Middle: $ns+np$ subsets. Bottom: $ns+np+nd$ subsets.

energy variation resulting in adding the $2p_\sigma$ orbital to the full ns orbitals set. The effect is most notable. Recall from Fig. 10 the nearly correct reproduction of the E state (not reported in Fig. 12 to save space) by addition of the $2p_\sigma$. The state $3a$ now closely approximates the first minimum of the H state (in the inset its curve can be hardly distinguished from the correct minimum). However, it must be also related to the minimum of state G, indeed, a new minimum appears just above H; therefore curve $3a$ is related to PEC GK. The $4a$, $5a$, and $6a$ curves are related to states H, P, and O, respectively. In this figure we plot the curves $7a$, $8a$, and $9a$ even if largely different from the PECs 7, 8, and 9. It is worth noting that with the inclusion of the $2p_\sigma$ orbital there are five curves well reproducing the first five excited states. Curves $2a$ and $3a$ dissociate as $H(1s)+H(2l)$, curve $4a$ as $H(1s)+H(3l)$, curve $5a$ as $H(1s)+H(4l)$, and curve $6a$ as $H(1s)+H(5l)$. The last two dissociation products are incorrectly reproduced at this stage.

The effect of the two $3p_\sigma$ STOs is considered in the middle inset of Fig. 12 (with the warning that some of the effects might be partly attributed to the long tail of the $2p_\sigma$ orbital). Curve $3a$ now follows closely the entire GK state energy and has no participation to the H state, the latter nicely reproduced by the $4a$ state. The $5a$, $6a$, and $7a$ curves are clearly related to the P, O, and 7 states, respectively. Curves $5a$ and $6a$ are close to each other and at about 2.7 bohr we can note a state crossing. The same situation holds for the curves $6a$ and $7a$, which cross once at 2.4 and a second time at 5.2 bohr. The curves $7a$, $8a$, and $9a$ are notably stabilized comparatively to their energy without the $3p_\sigma$ STOs. Curves $2a$ and $3a$ dissociate as $H(1s)+H(2l)$, curves $4a$ and $5a$ as $H(1s)+H(3l)$, and curves $6a$ and $7a$ as $H(1s)+H(4l)$. Note that the dissociation products of curve $6a$ are incorrectly reproduced.

The $2p_\pi$ effect complemented by that of the $3p_\pi$ and of the full np STO set is clearly visible in the bottom inset, where GK an H states are nicely reproduced by the $2a$, $3a$, and $4a$ curves. The PEC P is now reasonably well reproduced and the density analysis indicates a $(1s3p)$ configuration from 3.0 to 2.7 bohr. In addition, curves $5a$ to $8a$ are now all in a reasonable energy range. The remaining small disagreements and the notable disagreement for curves $9a$ and $10a$ between the correct PEC energy and the na curves are attributed to the absence of the nd functions, thus the $3d$ and the $4d$ and higher orbitals must be considered in order to obtain a satisfactory agreement for the H, P, and O states. Indeed, the density analysis for the H state indicates the presence of $(1s3d)$ configuration between 3.0 and 6.2 bohr, and for the O state the $(1s4d)$ configuration for distances shorter than 4.4 bohr.

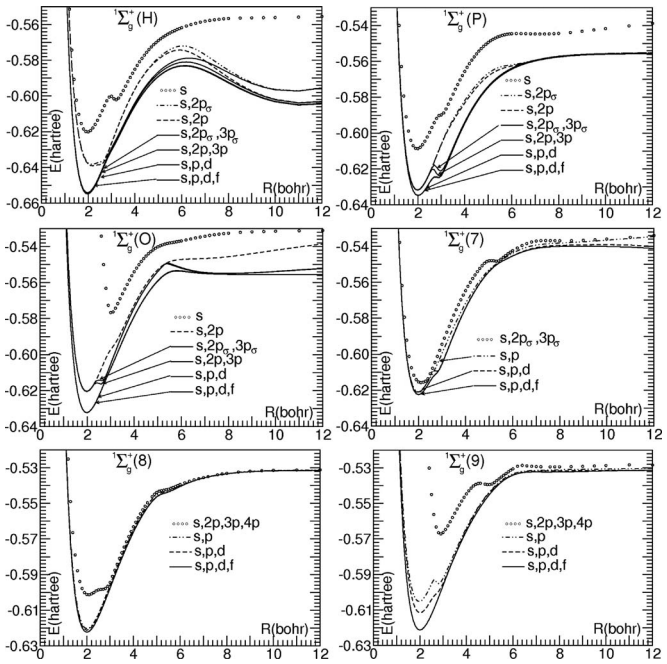

FIG. 14. Subset energy analysis for the states *H*, *P*, *O*, 7, 8, and 9.

The insets of Fig. 13 report the decomposition into *s*, *p*, and *d* subsets for the high excited states 7–14, since the *nd* subsets are dominant mainly for high excited states. In the top inset of Fig. 13 we report the curves for the *s* subset; curve 7*a* is the only one which presents a minimum with only *s* subsets. In the middle inset of Fig. 13 we present the curves up to 11*a* obtained by including the *s* and the *p* subsets: curves 7*a*, 8*a*, and 9*a* now closely follow the corresponding PECs, therefore poorly visible in the graph since superimposed to the final PEC values. Curves 10*a* and 11*a* appear clearly and present a well defined minimum. Finally the bottom inset of Fig. 13 reports the results with up to the *d* subset. Now curves 7*a*, 8*a*, and 9*a* follow very closely the PECs, curve 10*a* is close to PEC 12, and curve 12*a* is above PEC 13. The inclusion of the *f* functions yields the final PECs reported in Fig. 6.

The graphs of Figs. 11–13 are rather complex due to partial but frequent superposition of curves. Thus, in Fig. 14 these deficiencies are eliminated by considering the states *H*, *O*, *P*, 7, 8, and 9 one at the time (as previously done for the states *X*, *EF*, and *GK* in Fig. 10).The analysis of the insets is immediate simply by inspection and needs no comment.

This concludes the subset energy analysis of the PECs with identification step by step of specific contributions, thus yielding information on the dominant *nl* orbitals in each state for a given internuclear separation.

VIII. ANALYSIS OF THE ELECTRONIC DENSITY VIA COMPUTATION OF MOLECULAR DISTRIBUTION FUNCTIONS

In this section we systematically analyze the electronic density for the $^1\Sigma_g^+$ states comparing the molecular radial distribution functions on one H atom in the H_2 molecule, starting at large internuclear distances, 10 000 and 1000 bohr (where the distributions are those of the separated atoms), and progressively moving to shorter and shorter distances. In this section we use the molecular distribution function comparative method exposed in Sec. III. We sample (from the united atom to 10 000 bohr) the PECs particularly in proximity of energy minima and avoided state crossing and at other selected internuclear separations to identify and check on eventual variations in the molecular radial distribution functions. The sampling performed at about 30 internuclear distances yields a reasonably complete representation on the electronic density transformations concomitant with the molecular formation process.

The ground state at dissociation has the well known electronic density characterized by the radial distribution functions $D_{nl}(r)$ of two H[$^2S(1s^1)$] atoms (with radial distribution maximum at 1.0 bohr from the nucleus and the typical shape given in Fig. 3) which eventually transforms itself into the He[$^1S(1s^2)$] radial distribution at the united atom (with the maximum of the radial distribution function at 0.5 bohr from the He atom nucleus, see Fig. 1). In the density analysis, we follow the gradual transformations starting with the H[$^2S(1s^1)$] density of the two separated atoms at 10 000 bohr until about 10 bohr, where the two atoms are weakly interacting, then to shorter and shorter internuclear distances with the gradual overlap of the two atoms yielding the well known ground state density with two symmetric peaks in correspondence of the two H atom nuclear positions. Note that the molecular probability distribution $1(1s1s)$ yields very clearly the $1s$ as the prevailing orbital; the $2s$, $2p$, and $3d$ contributions are of secondary relevance.

Concerning the excited states, one H atom always dissociates as H[$^2S(1s^1)$] and the second as H(nl^1), as shown in Fig. 3, right insets. We start with the *EF* and the *GK* states for which *nl* is either the $(2s)$ or the nearly degenerate $(2p)$. We continue with the *H*, *P*, and *O* states, whose second H atom dissociates either into the H[$^2S(3s)$], H[$^2P(3p)$], or the H[$^2D(3d)$] nearly degenerate states. Finally, we analyze the states 7–10 for which one atom dissociates into the H[$^2S(4s)$], H[$^2P(4p)$], H[$^2D(4d)$], or H[$^2F(4f)$] states. Preliminary comments are added for the states 11–15 where one H atom dissociates as H[$^2S(1s^1)$] and the second as H($5l^1$).

Our comparative analysis assigns the *EF* state electronic density at dissociation (R=10 000–1000 bohr) to $2(1s2p)$, namely, H[$^2S(1s^1)$] and H[$^2P(2p^1)$]; at 100 bohr there is a switch to the $(1s2s)$ configuration with a very small energy stabilization. Approaching R=20 bohr the density changes into a mixture of $(1s2s)$ and $(1s'1s')$ configurations, where the $1s'$ denotes the orbital of the ionic $H^+H^-[1s'1s']$ state. Recall that the H^+H^- system has radial distributions which extend at notably larger distances relative to those of H_2 (see Fig. 3). In the regions 15–30 the ionic component is large (see the top inset Fig. 9). At 3.0 bohr (in the region of the energy barrier separating the *E* and *F* minima) we find again a $(1s2s)$ predominant configuration and no ionic contribution; this situation persists until 0.4 bohr as verified by analyzing the intermediate molecular radial distributions at 2.9, 2.8, 2.7, 2.0, 1.9, 1.1, 1.0, and 0.9 bohr. At the united atom the configuration is He[$^1S(1s2s)$]. The above detailed analysis confirms recent studies.[24,25]

For the state *GK*, at R=10 000 bohr we observe the

$H[1s]+H[2s]$ configuration. At $R=100$ bohr there is a switch to the $(1s2p)$ configuration, which persists until about 2.9 bohr (near the barrier point). From here until 1.1 bohr the $(1s3d)$ configuration dominates, then it changes into $(1s3s)$. From 1.0–0 bohr the distribution approaches more and more the one of $He[1s3s]$.

We consider now the H, P, and O states which dissociate as $(1s3d)$, $(1s3p)$, and $(1s3s)$, respectively. The electronic configuration $(1s3d)$ of the state H persists until about 30 bohr, where it switches to the ionic $(1s'1s')$ configuration, the latter persisting until about 7.0 bohr (see Fig. 9). From about 6.2–3.0 bohr the configuration is $(1s3d)$ and it becomes $(1s3s)$ from 2.9–1.1 bohr. At $R=1.0$ bohr the configuration is $(1s3d)$ and becomes $He[^1D(1s3d)]$ at the united atom. The crossing in the region 1.0–1.1 bohr between states GK and H is confirmed by the switch in their electronic configurations.

The state P at $R=10\,000$ bohr dissociates as $H[1s]+H[3p]$ and remains $(1s3p)$ until 60 bohr. From 30–10 bohr the configuration is $(1s3d)$ then becomes $(1s3s)$ until 3.3 bohr. In the interval of 3.0–2.7 bohr the main characterization is $(1s3p)$. From 2.0–1.1 bohr the density analysis leads to $(1s4d)$ and at 1.0 bohr we note a change into $(1s4s)$ leading to the $He[^1S(1s4s)]$ at the united atom.

The state O at $R=10\,000$ bohr dissociates as $H[1s]+H[3s]$ and remains this way until 60 bohr; at 30 bohr it becomes $(1s3p)$ and remains in this configuration until 5.8 bohr. From 4.4–2.9 bohr the configuration is $(1s4d)$. From 2.8–1.1 bohr it is $(1s4s)$; at 1.0 bohr it switches into a $(1s4d)$ density like the one for $He[^1D(1s4d)]$. The crossing in the region 1.0–1.1 bohr between states P and O is confirmed by the switch in their electronic configurations.

For the above states, EF to O, the identification is clear with no problem in differentiating the n and l values.

For the states 7–10 the configurations are formed with atomic orbitals with relatively high nl values, thus the molecular distribution functions present several maxima and minima, often overlapping and near in energy, thus making the assignments somewhat difficult.

With this in mind let us consider the electronic density evolution for the state 7. At 10 000 bohr the configuration is $H_2[1s4d]$ which transforms into an ionic configuration from 100–15 bohr, where it switches to $(1s3d)$ until about $R=5.8$ bohr. After a few switches between $(1s4p)$ and $(1s4s)$ at 1.1 bohr it is $(1s5d)$ and at 1.0 bohr it goes into the $He[1s5s]$ configuration (see Figs. 5 and 7).

State 8 starts at 10 000 bohr as $H_2[1s4f]$; at 100 bohr it is $(1s4d)$ and persists this way until 60 bohr, then the configuration becomes $(1s3s)$. At $R=7.0$ bohr the configuration is $(1s4s)$ then switches into $(1s5d)$ and $(1s5s)$ to finally merge at 1.0 bohr into $He[^1D(1s5d)]$.

State 9 starts at 10 000 bohr as $H_2[1s4p]$ then switches a number of times into the $(1s4d)$ and $(1s4s)$ configurations until $R=4.4$ bohr. In the interval of internuclear distances between 4.4 and 2.8 bohr the configuration is initially $(1s5s)$, then $(1s5p)$ and $(1s5d)$. At shorter internuclear distances the configuration is $(1s4l)$, most likely $(1s4f)$, then $(1s6d)$, which finally merges into the united atom $He[^1S(1s6s)]$. In conclusion, the overall characterization of state 9 is that it starts at dissociation with $(1s4p)$ configuration, which transforms into $(1s5l)$ and then into $(1s6l)$ configurations, and finally into $He[^1S(1s6s)]$.

State 10 from $R=10\,000$ to about 3.3 bohr alternates between $(1s4s)$, $(1s4p)$, and $(1s4f)$; at 2.9 bohr it is $(1s5d)$, then at 2.0 bohr it becomes $(1s6s)$ and finally merges into $He[^1D(1s6d)]$. State 11 from $R=10\,000$ to about 10 bohr is characterized by an ionic configuration. At shorter distances one after the other there are evidence for the $(1s4l)$, then $(1s5l)$ and $(1s6l)$, converging eventually to $He[^1S(1s7s)]$.

The density variations above detected are expected to persist when vibrations and rotations and time dependence are explicitly considered, thus are expected to characterize the H_2 molecular interactions.

IX. CONCLUSIONS

The H_2 $^1\Sigma_g^+$ state manifolds with electronic configuration $1s^1nl^1$ $(n=1-5$ and $l=0-3)$ are studied from $R=0.01$ to 10 000 bohr with realistic quantum mechanical energy computations and, for the first time, with a comprehensive and detailed energy and density analyses. Previous studies were limited to the ground state and/or to the first few excited states.

The energies are obtained from full CI computations with extended and optimized STO and GTO basis sets using both HF and HL orbitals. The reliability of our PEC computations is verified by comparing with the best energies in the H_2 literature:[19,21] our average energy deviations are between 10^{-5} and 10^{-4} hartree from the best computed values. Equivalent accuracy is expected for the computations of the states 7–10, resulting from the parallel computations with STO and GTO; thus our analyses are based on realistic wave functions and energy data. We report, in addition, the preliminary computations and analyses for the state 11 which dissociates as H^+H^- and states 12–15 which dissociate as $H(1s)+H(5l)$.

The total energies are quantitatively analyzed in terms of covalent and ionic contributions, and the IEP is quantitatively determined for each state from computations of the total energy and its covalent component. Thus, the energy decompositions, in particular, the energy of the ionic component, have an unambiguous foundation. Related systems He, H^-, H^+H^- ion pair, and the proton H^- are computed with full CI and analyzed to assist in the characterization of the H_2 molecule from united atom to dissociation.

For each $n>1$ value, there is always one state which interacts with the H^+H^- system. This leads to a second minimum at an internuclear separation that increases with increasing value of n. Indeed, we observe a strong ionic character for states EF, H, 7, and 11, which dissociate as $H(1s)+H(2s)$, $H(1s)+H(3d)$, $H(1s)+H(4d)$, and H^+H^-, respectively. From preliminary computations, this finding extends also to the $^1\Sigma_u^+$ state manifold.[54]

The complexity of the PECs parallels the multiple and complex transformations occurring in the electronic density from large distances to the united atom. The electronic density evolution leading to the multiple minima and the occurrence of the many state crossing is analyzed following the

variations in the molecular distribution functions from united atom to dissociation and the effect of decomposing the full basis set into subsets.

ACKNOWLEDGMENTS

One of us (G.C.) acknowledges a grant from MIUR (Grant No. 2006030944).

[1] G. Herzberg, *Molecular Spectra and Molecular Structure. Spectra of Diatomic Molecules* (Van Nostrand, Princeton, 1950), Vol. 1.
[2] K. P. Huber and G. Herzberg, *Molecular Spectra and Molecular Structure IV. Constants of Diatomic Molecules* (Van Nostrand, Princeton, 1979).
[3] A. de Lange, W. Hogervorst, W. Ubachs, and L. Wolniewicz, Phys. Rev. Lett. **86**, 2988 (2001).
[4] E. Reinhold, W. Hogervorst, W. Ubachs, and L. Wolniewicz, Phys. Rev. A **60**, 1258 (1999).
[5] W. Heitler and F. London, Z. Phys. **44**, 455 (1927).
[6] R. S. Mulliken, Phys. Rev. **32**, 186 (1928) (and references therein).
[7] E. A. Hylleraas, Z. Phys. **48**, 469 (1928).
[8] D. R. Hartree, Proc. Cambridge Philos. Soc. **24**, 89 (1928).
[9] A. D. McLean, A. W. Weis, and M. Yoshimine, Rev. Mod. Phys. **32**, 211 (1960).
[10] W. Kolos and C. C. J. Roothaan, Rev. Mod. Phys. **32**, 219 (1960).
[11] H. M. James and H. A. Coolidge, J. Chem. Phys. **1**, 825 (1933).
[12] H. M. James, H. A. Coolidge, and R. D. Present, J. Chem. Phys. **4**, 193 (1936).
[13] E. R. Davidson, J. Chem. Phys. **35**, 1189 (1961).
[14] W. Kolos and L. Wolniewicz, J. Chem. Phys. **41**, 3663 (1964).
[15] W. Kolos and L. Wolniewicz, J. Chem. Phys. **43**, 2429 (1965).
[16] W. Kolos and L. Wolniewicz, J. Chem. Phys. **45**, 509 (1966).
[17] W. Kolos, J. Chem. Phys. **101**, 1330 (1994).
[18] L. Wolniewicz, J. Chem. Phys. **99**, 1851 (1993).
[19] L. Wolniewicz and K. Dressler, J. Chem. Phys. **100**, 444 (1994).
[20] L. Wolniewicz, J. Chem. Phys. **103**, 1792 (1995).
[21] L. Wolniewicz, J. Chem. Phys. **108**, 1499 (1998).
[22] G. Staszewska and L. Wolniewicz, J. Mol. Spectrosc. **212**, 208 (2002).
[23] T. Detmer, P. Schmelcher, and L. S. Cederbaum, J. Chem. Phys. **109**, 9694 (1998).
[24] J. Wang, J. M. Mercero, I. Silanes, and J. M. Ugalde, Europhys. Lett. **76**, 808 (2006).
[25] J. Wang, Y. Wang, S. Lv, and J. M. Ugalde, J. Chem. Phys. **127**, 074307 (2007).
[26] M. Tachikawa, K. Teneda, and K. Mori, Int. J. Quantum Chem. **7**, 547 (1992).
[27] M. Tachikawa and Y. Osamura, J. Chem. Phys. **113**, 4942 (2000).
[28] M. Stenrup, A. Larson, and N. Elander, Phys. Rev. A **79**, 012713 (2009).
[29] R. S. Mulliken, J. Am. Chem. Soc. **88**, 1849 (1966).
[30] M. O. Vieitez, T. I. Ivanov, E. Reinhold, C. A. de Lange, and W. Ubachs, Phys. Rev. Lett. **101**, 163001 (2008).
[31] W. A. Chupka, P. M. Dehmer, and W. T. Jivery, J. Chem. Phys. **63**, 3929 (1975).
[32] R. C. Shiell, X. K. Hu, Q. C. J. Hu, and J. W. Hepburn, Faraday Discuss. **115**, 331 (2000).
[33] E. Reinhold and W. Ubachs, Phys. Rev. Lett. **88**, 013001 (2001).
[34] E. Clementi and G. Corongiu, Int. J. Quantum Chem. **108**, 1758 (2008).
[35] C. Froese Fischer, At. Data Nucl. Data Tables **4**, 301 (1972).
[36] F. Sasaki and M. Yoshimine, Phys. Rev. A **9**, 17 (1974).
[37] J. C. Browne and R. D. Poshusta, J. Chem. Phys. **36**, 1933 (1962).
[38] E. Hylleraas, Z. Phys. **71**, 739 (1931).
[39] J. K. L. MacDonald, Proc. R. Soc. London, Ser. A **136**, 328 (1932).
[40] A. Wilson, D. E. Woon, K. A. Peterson, and T. H. Dunning, Jr., J. Chem. Phys. **110**, 7667 (1999).
[41] J. Fernandez Rico, R. Lopez, I. Ema, and G. Ramirez, J. Comput. Chem. **25**, 1987 (2004).
[42] G. Corongiu, J. Phys. Chem. A **111**, 5333 (2007).
[43] G. Corongiu, J. Phys. Chem. A **111**, 13611 (2007).
[44] C. E. Moore, *Atomic Energy Levels*, NBS Circular 467 Vol. 1 (U.S. Government Printing Office, Washington, DC, 1971).
[45] L. Pauling and E. B. Wilson, *Introduction to Quantum Mechanics* (McGraw-Hill, New York, 1935).
[46] J. C. Slater, J. Chem. Phys. **19**, 220 (1951).
[47] L. Pauling, *The Nature of the Chemical Bond* (Cornell University Press, Ithaca, 1960).
[48] C. L. Pekeris, Phys. Rev. **112**, 1649 (1958).
[49] E. R. Davidson, in *Physical Chemistry, Electronic Structure of Atoms and Molecules*, edited by D. Henderson (Academic, New York, 1969), Vol. III.
[50] E. Wigner and E. E. Witmer, Z. Phys. **51**, 859 (1928).
[51] R. S. Mulliken, Rev. Mod. Phys. **4**, 1 (1932).
[52] L. Wolniewicz, J. Chem. Phys. **109**, 2254 (1998).
[53] S. Yu and K. Dressler, J. Chem. Phys. **101**, 7692 (1994).
[54] G. Corongiu and E. Clementi J. Phys. Chem. (in press).